New Insights into Wideband Synthetic Aperture Radar Interferometry

Victor Mustieles-Perez, Sumin Kim, *Member, IEEE*, Gerhard Krieger, *Fellow, IEEE*, and Michelangelo Villano, *Senior Member, IEEE*

***Abstract*— Synthetic aperture radar interferometry (InSAR) is a technique that exploits the phase difference between two synthetic aperture radar (SAR) images to generate digital elevation models (DEMs) of the imaged terrain. InSAR has a well-established theoretical background, but approximations for narrowband signals are often made. To unwrap the interferometric phase, dual-baseline techniques are also commonly employed. Modern InSAR systems will use wider bandwidths to improve the accuracy and resolution of the DEMs. This letter generalizes the expressions of the baseline decorrelation and the critical baseline for InSAR systems with wide bandwidths and large baselines, where the spectral shrinkage is not negligible. It is also shown that radargrammetry offers high potential to unwrap the interferometric phase already on a pixel-by-pixel basis. The proposed approach can also exploit acquisitions with multiple baselines or frequency bands. The results show that a single wideband interferometric acquisition may suffice to perform phase unwrapping for high interferometric coherences. The concepts discussed in this paper will help to design and enhance the performance of future wideband and multi-band InSAR missions to deliver a new generation of DEMs with unprecedented resolution and accuracy.**

***Index Terms*—Synthetic aperture radar (SAR), SAR interferometry, wide bandwidth, interferometric coherence, multi-band, unmanned aerial vehicle (UAV), drones, spectral shift, radargrammetry.**

I. Introduction

A CROSS-TRACK synthetic aperture radar (SAR) interferometry (InSAR) is a technique that combines two SAR images of the same scene acquired from different positions to extract the phase difference and form a digital elevation model (DEM) of the observed terrain [1], [2]. Conventional InSAR systems such as TanDEM-X are characterized by a range bandwidth much smaller than the carrier frequency (a few percent in the case of TanDEM-X) and are therefore considered as narrowband InSAR systems [3].

InSAR acquisitions with larger geometric baselines can yield DEMs with improved accuracy due to a smaller scaling factor between the interferometric phase and the terrain topography, which is often defined as the height of ambiguity h_{amb}. For distributed scatterers, however, the interferometric coherence between the SAR images degrades with increasing baseline due to baseline and volume decorrelation, which adversely affect the performance of large-baseline interferograms. This baseline decorrelation can be avoided by filtering the signals to a common range frequency band at the expense of resolution degradation, which also reduces the available number of looks [4], [5]. Therefore, a trade-off between the height of ambiguity and the interferometric coherence is required.

Future InSAR systems will make use of wider bandwidths and hence enable larger baselines. This is supported by the new regulation adopted by the International Telecommunication Union (ITU) in 2015, which allows using a bandwidth of up to 1200 MHz at X-band. High-resolution wide-swath (HRWS) is an example of a X-band SAR mission proposal which makes use of such bandwidth [6]. Airborne systems such as DLR's F-SAR allow multi-band InSAR measurements at X-band and S-band [7]. Furthermore, recent works have shown that unmanned aerial vehicles (UAVs) or drones can be equipped with radars with very large fractional bandwidth, i.e., the ratio between the radar bandwidth and center frequency [8]. Approximations for narrowband systems are usually considered in the InSAR theory. InSAR systems with wide fractional bandwidth enable improved performance, but require a revision of some theoretical points. This letter addresses two key aspects of wide-fractional-bandwidth InSAR.

The first aspect concerns InSAR baseline decorrelation for wide fractional bandwidth, which is especially important in systems using large baselines. The proposed model considers not only the spectral shift, but also its shrinkage, i.e., the frequency-dependent spectral shift within the system bandwidth, and allows accurate coherence modeling and improved DEM performance regardless of the system bandwidth and baseline [2], [9].

The second aspect concerns the phase unwrapping of an interferogram formed from wideband SAR images. Phase unwrapping can be performed using at least two interferograms with different baselines, as in the dual-baseline technique used

This paragraph of the first footnote will contain the date on which you submitted your paper for review, which is populated by IEEE. This work was partially funded by the Deutsche Forschungsgemeinschaft (DFG, German Research Foundation) GRK 2680 – Project-ID 437847244. Co-funded by the European Union (ERC, DRITUCS, 101076275). Views and opinions expressed are however those of the authors only and do not necessarily reflect those of the European Union or the European Research Council Executive Agency. Neither the European Union nor the granting authority can be held responsible for them. *(Corresponding author: Victor Mustieles-Perez).*

Victor Mustieles-Perez and Gerhard Krieger are with the Institute of Microwaves and Photonics (LHFT), Friedrich-Alexander University Erlangen-Nürnberg (FAU), 91058 Erlangen, Germany, and also with the Microwaves and Radar Institute, German Aerospace Center (DLR), 82234 Weßling, Germany (e-mail: victor.mustieles@dlr.de).

Sumin Kim and Michelangelo Villano are with the Microwaves and Radar Institute, German Aerospace Center (DLR), 82234 Weßling, Germany.

Color versions of one or more of the figures in this article are available online at http://ieeexplore.ieee.org

by TanDEM-X [10]. As an alternative, we propose to use radargrammetry on the same InSAR data to perform pixel-based phase unwrapping, as its absolute height measurements have an accuracy comparable to that of InSAR in wideband systems [11]. Radargrammetry was used for phase unwrapping in TanDEM-X only to some extent due to its limited height accuracy with narrowband signals [10], [12]. Therefore, a fundamental advantage of our approach is that it can be integrated very efficiently with InSAR due to the high commonalities between both processing chains, i.e., the radargrammetric shifts are computed in the coregistration stage.

II. Decorrelation Due to the Geometric Baseline

A. Geometric Decorrelation and Critical Baseline

The geometric or baseline decorrelation γ_{Rg} is a contribution to the interferometric coherence loss caused by the difference in the incidence angles of the master and slave acquisitions, θ_1 and θ_2, when a scene with distributed scatterers is imaged. Let us consider the InSAR acquisition geometry represented in Fig. 1, where P_i is the position of the i-th SAR acquisition and the subscript $i \in \{1, 2\}$ is the index of the radar platform. In the figure, r_i, H_i, θ_i, $\Delta\theta$, and β, denote the slant-range, platform altitude, incidence angle, interferometric angle and angle between platforms, respectively. The baseline B is decomposed into the parallel and perpendicular components, $B_\parallel$ and $B_\perp$.

In the case of repeat-pass InSAR, it can be observed that the terrain reflectivity is shifted in frequency by $2\pi f_0 \sin\theta_i$ and the bandwidth is stretched by a factor of $1/\sin\theta_i$, where f_0 denotes the center frequency of the radar signal [13]. Analogously, in the case of single-pass bistatic InSAR, the terrain reflectivity is shifted by $2\pi f_0(\sin\theta_1 + \sin\theta_2)/2$ and stretched by a factor of $2/(\sin\theta_1 + \sin\theta_2)$. The shrinkage of the spectra can only be neglected for narrowband signals. Under the assumption that $\theta_1 > \theta_2$, a shift factor ϑ between the two SAR signals can be defined as

$$\vartheta_{repeat} = \frac{\sin\theta_1}{\sin\theta_2} \tag{1}$$

for the case of repeat-pass interferometry and as

$$\vartheta_{single} = \frac{2}{1+1/\vartheta_{repeat}} \tag{2}$$

for the case of single-pass interferometry. The frequency shift and bandwidth shrinkage are equivalent to a model that projects the imaged frequencies of the transmitted spectra on the ground [2], [5]. Thus, γ_{Rg} can be computed considering the common and non-common spectral parts, which yields:

$$\gamma_{Rg} = \frac{1}{B_F}\left[\frac{2+B_F}{1+\vartheta} - \frac{2-B_F}{1+1/\vartheta}\right], \tag{3}$$

for baselines smaller than $B_{\perp,crit}$, where $B_F = B_{Rg}/f_0$ is the fractional bandwidth of the system, being B_{Rg} the radar bandwidth, and ϑ is the shift factor determined by (1) or (2) depending on the acquisition mode [5], [13], [14]. If $\Delta\theta$ is small, the parallel ray approximation holds and (3) yields the linear geometric decorrelation expression used in spaceborne scenarios, in which the single- and repeat-pass expressions only differ by a factor of 2 [2]. The critical baseline $B_{\perp,crit}$ may be then derived from (3) by assuming $\gamma_{Rg} = 0$ and solving for $B_\perp$. The shift factor at the critical baseline is given by

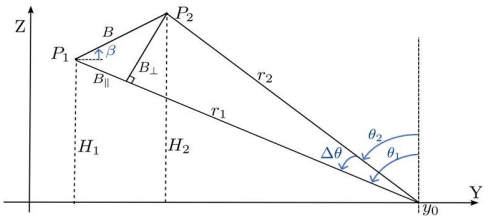

Fig. 1. Geometry of across-track InSAR acquisition in the zero-Doppler plane.

$$\vartheta_{crit} = \frac{2+B_F}{2-B_F}. \tag{4}$$

Considering also that the interferometric angle is given by

$$\Delta\theta = \arctan\left(\frac{B_\perp}{r_1 - B_\parallel}\right), \tag{5}$$

$B_{\perp,crit}$ can be approximated as follows

$$B_{\perp,crit} \approx \frac{r_1}{\tan(\theta_1-\beta) + \frac{1}{\tan\left(\theta_1 \frac{m \cdot B_F}{1+B_F/2}\right)}}, \tag{6}$$

with $m = 1, 2$ for repeat- and single-pass InSAR, respectively. γ_{Rg} has been evaluated from simulated radar data, generated through InSAR acquisitions over a uniform, surface-like scene modelled using numerous point scatterers as detailed in [15], and compared with the narrow- and wideband models. Fig. 2 depicts, for the case of repeat-pass InSAR, the predicted γ_{Rg}, $B_{\perp,crit}$ and the recovered coherence after filtering, evaluated using the conventional and the proposed models with dashed and solid lines, respectively. The curves for the case of single-pass InSAR are similar but considering baselines approximately twice as large. Fig. 2 (a) shows the predicted γ_{Rg} with respect to the ratio $B_\perp/B_{\perp,crit}$, calculating $B_{\perp,crit}$ using (6) and assuming $B_F = 10\%$ (orange) and $B_F = 100\%$ (blue). The conventional model notably underestimates γ_{Rg} for wide fractional bandwidths and large baselines. Fig. 2 (b) compares $B_{\perp,crit}$ calculated using the conventional formula and (6). The former gives values larger than using (6) by a factor of 1.25, 1.55 and 1.9 at fractional bandwidths of 20%, 40%, and 60%, respectively. The values of the coherence and the critical baseline obtained with (3) and (6), respectively, agree with the simulations. If we consider a UAV-based wideband InSAR system with $B_F = 100\%$ and $B_\perp = 0.2\, B_{\perp,crit}$, the wideband model leads to $\gamma_{Rg} \approx 0.65$, while the conventional model yields a value of 0.8, therefore overestimating the performance. The failure of the conventional narrowband approximation can also become significant for wideband coherence SAR tomography and can lead to a baseline-dependent discrepancy between the measured and expected coherences.

B. Modified Spectral Filtering for Wideband SAR Signals

The state-of-the art filters to avoid baseline decorrelation only consider a spectral shift. The spectral shrinkage, however, also needs to be accounted for in the wideband case [5]. The wideband definition of the filters to bring the signals to a common band in range is directly derived from (1) and (2) to remove the non-common spectra of the InSAR pair, yielding:

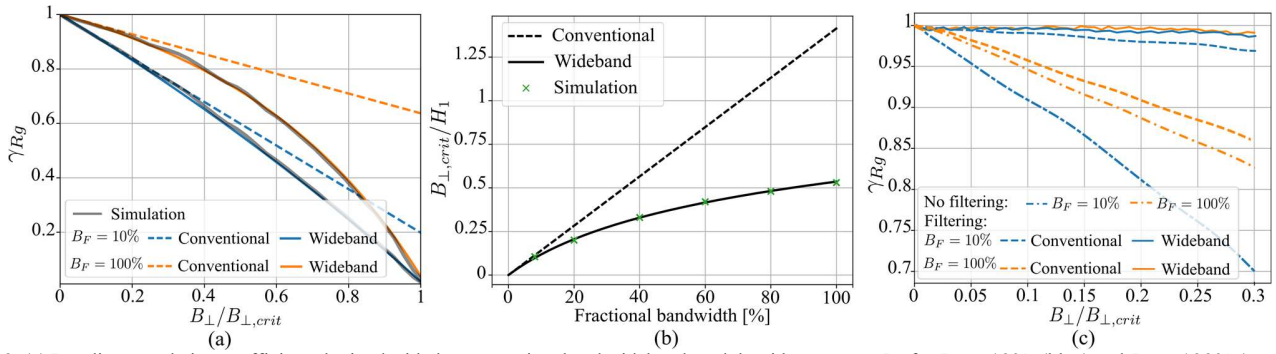

Fig. 2. (a) Baseline correlation coefficient obtained with the conventional and wideband models with respect to $B_\perp$ for $B_F = 10\%$ (blue) and $B_F = 100\%$ (orange). (b) Critical baseline obtained with the conventional (dashed) and wideband (solid) models versus B_F. (c) Simulated baseline correlation coefficient without filtering (dash-dotted) and after filtering with the conventional (dashed) and the wideband (solid) filters for $B_F = 10\%$ (blue) and $B_F = 100\%$ (orange).

$$\begin{cases} W_{f1} = \frac{f_0}{2}\left[(2+B_F)\frac{1}{\vartheta} - (2-B_F)\right], \\ f_{o,f1} = \frac{f_0}{4}\left[(2+B_F)\left(\frac{1}{\vartheta}-1\right)\right] \end{cases} \tag{7}$$

$$\begin{cases} W_{f2} = \frac{f_0}{2}[(2+B_F) - (2-B_F)\cdot\vartheta], \\ f_{o,f2} = \frac{f_0}{4}[(2-B_F)(\vartheta-1)] \end{cases} \tag{8}$$

where W_{fi} and f_{0,f_i} denote the bandwidth and central frequency of each filter, respectively [13]. The filters depend on θ_i and have to be adapted depending on the topography, which can be estimated, e.g., from an external DEM or a coarser DEM obtained from a preliminary processing of the data, and range like in their narrowband definition [5]. The two filtered SAR images contain the same portion of the ground reflectivity spectrum. Due to the different incidence angles, the resolution and bandwidth of the filtered SAR images in slant range are different. The difference in bandwidth is negligible only in narrowband systems because $\Delta\theta$ is small. Fig. 2 (c) shows γ_{Rg} measured from filtered data, where the dashed and solid lines depict the results using the conventional and wideband filters, respectively. The proposed wideband filters fully recover the coherence as they are perfectly adapted to the common bandwidth, while the state-of-the-art filters intended for narrowband signals are less effective for wide fractional bandwidths and large baselines [5]. The effect of the spectral shrinkage results to be still small for systems with $B_F = 10\%$. Discrepancies become significant from $B_F = 30\%$, especially regarding the calculation of $B_{\perp,crit}$. The recovered γ_{Rg} is not strictly 1 mainly due to residual coregistration errors.

III. Phase Unwrapping Using Radargrammetry

Radargrammetry was used in the TanDEM-X mission to detect phase unwrapping errors and calibrate the DEMs to absolute heights. Nevertheless, because of the low height accuracy of radargrammetry for narrowband signals, averaging of many resolution cells over large areas was necessary [10], [12]. In the following, it is shown that radargrammetry can be used in wideband and multi-band InSAR systems for phase unwrapping at a much smaller scale. This analysis considers the case of fully developed speckle, while the presence of features in the SAR images can further improve the shift estimation and thus the height accuracy of the radargrammetric DEM [16]. The Cramer-Rao lower bound on the standard deviation of the height accuracies of InSAR $\sigma_{h,InSAR}$ and radargrammetry $\sigma_{h,rad}$ are given, respectively, by:

$$\sigma_{h,InSAR} = \left(\frac{\lambda}{2}\cdot\frac{r_1\sin\theta_1}{B_\perp}\cdot\frac{1}{2\pi}\right)\cdot\frac{1}{\gamma}\frac{\sqrt{1-\gamma^2}}{\sqrt{2N}} \tag{9}$$

and

$$\sigma_{h,rad} = \left(\frac{c}{2B_{Rg}}\cdot\frac{r_1\sin\theta_1}{B_\perp}\right)\cdot\sqrt{\frac{3}{2N_c}}\frac{\sqrt{1-\gamma^2}}{\pi\gamma}osf^{3/2}, \tag{10}$$

where N denotes the multi-looking factor, N_c is the size of the estimation window, γ is the interferometric coherence, and osf is the range oversampling factor [4], [11]. The second part of (9) and (10) represents the Cramer-Rao lower bound on the standard deviation of the estimate of the InSAR phase and the radargrammetric shift, respectively. The two height estimates are compared assuming a sufficient number of looks so that no interferometric phase wrapping occurs. The ratio between the height accuracies of radargrammetry and InSAR results in

$$\frac{\sigma_{h,rad}}{\sigma_{h,InSAR}} = \frac{1}{B_F}\cdot 2\sqrt{3}\cdot osf^{\frac{3}{2}}. \tag{13}$$

The height accuracy of radargrammetry approaches that of InSAR when B_F increases because the scaling factor between the radargrammetric shift and the topographic height decreases with B_{Rg}. However, the maximum possible B_F is 2, hence, $\sigma_{h,rad}$ never reaches $\sigma_{h,InSAR}$ according to (13) in the limit of a sufficient number of looks. Fig. 3 (a) shows the expected performance of InSAR and radargrammetry with respect to B_F, assuming $B_\perp = 0.1\cdot B_{\perp,crit}$, $\theta_1 = 45^o$, $\gamma = 0.8$, and $N = N_c = 12$. The performance difference between both methods is reduced due to sensitivity term although never equal.

While interferometry outperforms radargrammetry, their performance is comparable in wideband systems, and hence, radargrammetry can be exploited to support phase unwrapping when $\sigma_{h,rad} < h_{amb}$. The ratio between $\sigma_{h,rad}$ and h_{amb} in the case of equal acquisition configurations is given by

$$\frac{\sigma_{h,rad}}{h_{amb}} = \frac{1}{B_F}\sigma_{\Delta\hat{x}}, \tag{14}$$

where $\sigma_{\Delta\hat{x}}$ is the standard deviation of the radargrammetric shift estimate. This quantity is depicted in Fig. 3 (b) with respect to B_F, it results to be lower than 1 for $B_F > 10\%$. Considering the parameters of the HRWS mission, Fig. 3 (b) shows that radargrammetry is a promising solution for phase unwrapping in future wideband InSAR missions in X-band [6].

A fundamental advantage of using radargrammetry for phase

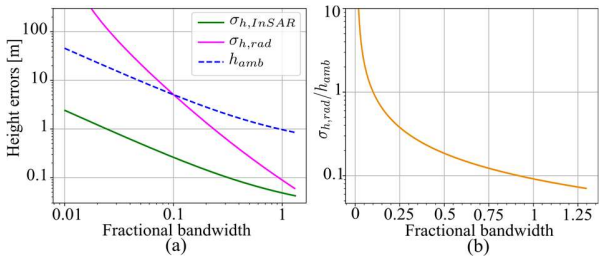

Fig. 3. (a) Height accuracy of interferometry and radargrammetry, and height of ambiguity as a function of the fractional bandwidth of the system for $\gamma = 0.8$, and $N = N_c = 12$. (b) Ratio $\sigma_{h,rad}/h_{amb}$ versus the fractional bandwidth.

unwrapping is its high commonality with conventional InSAR processing, since the shifts between SAR images are computed in the coregistration stage. Radargrammetric measurements can also be used to calibrate the DEM to the absolute terrain height.

A. Phase Unwrapping in Wideband Systems

The proposed approach to perform phase unwrapping uses an absolute DEM obtained by radargrammetry to pixelwise detect and correct phase unwrapping errors in the DEM generated using interferometry. A phase unwrapping error is detected if the difference between the DEMs from InSAR and radargrammetry is larger than $h_{amb}/2$. Upon detection of a phase unwrapping error, the height is corrected as

$$h_{final} = h_{InSAR} + \left\lfloor \frac{h_{rad} - h_{InSAR}}{h_{amb}} \right\rceil h_{amb} \qquad (15)$$

where h_{InSAR} and h_{rad} denote the heights of the DEMs from InSAR and radargrammetry, respectively, and h_{final} is the corrected height. A very low probability of phase unwrapping errors is needed in the considered pixelwise approach, i.e., $\sigma_{h,rad}/h_{amb} < 1/6$ for a correct unwrapping in around 99.7% of the cases [10]. Post-processing techniques that exploit surrounding pixels might further relax this requirement in the pixelwise approach. According to (14), phase unwrapping can be effectively performed with a single-baseline acquisition if B_F is sufficiently large. Furthermore, $\sigma_{h,rad}$ can be improved by increasing N_c or averaging estimations, nevertheless the resolutions of the DEMs from radargrammetry and interferometry should be kept at a similar scale.

When the requirement on the probability of phase unwrapping errors cannot be met, a second acquisition with a smaller baseline can be used. In this case, the DEM from radargrammetry obtained with the large baseline is used to correct the phase unwrapping errors in the small-baseline DEM formed using InSAR. The small-baseline DEM obtained with InSAR is then used to correct phase unwrapping errors in the large-baseline DEM. The proposed approach is applied to simulated radar data generated with different acquisition parameters to evaluate its phase unwrapping performance. The radar data were again generated through repeat-pass InSAR acquisitions over a uniform scene modelled using numerous point scatterers [15]. The probability of unwrapping errors is computed as the ratio of the number of simulated DEM pixels where $|h_{rad} - h_{true}| > h_{amb}/2$, being h_{true} the true terrain height, to the total number of simulated pixels. Fig. 4 (a) shows for the proposed dual-baseline approach the probability of residual phase unwrapping errors for multiple values of B_F and γ. 5 looks are assumed in both azimuth and range. This corresponds to a DEM resolution (or posting) of 0.25 m in azimuth and 0.35 m in ground range, assuming $B_{Rg} = 3$ GHz, $\theta_1 = 45°$ and no slope. The baseline ratio is chosen according to the red line in Fig. 4 (b), which minimizes the probability of unwrapping errors with respect to B_F, while a large baseline equal to $0.1 \cdot B_{\perp,crit}$ is used. The dashed and dotted lines in Fig. 4 (a) indicate where the single-baseline approach would allow a probability of phase unwrapping errors of 1% and 0.1%, respectively, and hence illustrate the boundary of the regions where phase unwrapping may be performed with one or two InSAR acquisitions, as indicated by the two arrows. The results show that less than 1% unwrapping errors can be achieved with radargrammetry considering a second baseline with $B_F > 10\%$ and $\gamma > 0.6$, and hence the proposed approach is a promising technique for future spaceborne wideband InSAR missions.

While the discussed case concerns two InSAR acquisitions which are obtained separately, three platforms in a single pass or three repeat-pass monostatic acquisitions can be used as well.

B. Phase Unwrapping in Multi-Band Systems

Performing multi-baseline InSAR acquisitions is costly, while using acquisitions in different frequency bands is another option to relax the condition in (14). This strategy is in line with many future SAR missions using multi-band SAR to investigate diverse natural processes simultaneously, e.g., the F-SAR, UAV-based systems or NASA-ISRO SAR [7], [8], [17].

A system operating at two frequency bands is assumed, the upper band is used to form the final accurate DEM, while the lower band is used to create an easier-to-unwrap interferogram. The DEM from InSAR in the lower frequency band is used as an intermediate step similarly to the discussed dual-baseline approach. The lower-band InSAR acquisition has potentially a smaller bandwidth but the same baseline as the upper-band one, nevertheless, $B_{\perp,crit}$ depends on B_F , whose variation is reasonable to be smaller. The number of looks in each frequency band is chosen to keep similar resolutions between the respective DEMs. Fig. 4. (c) shows the simulated probability of unwrapping errors with respect to γ and B_F. The fractional bandwidth of the lower frequency band B_F' is assumed to be 20%. The chosen ratio between the upper f_c and lower band f_c' center frequencies follows a similar trend to the ratio between baselines, depicted in Fig. 4 (b). The different ground penetration in each frequency band is modeled by assuming for the volume representing the soil a vertical exponential reflectivity profile, whose extinction coefficient is calculated from the permittivities measured by Hallikainen for a slightly moisturized clayey soil [18]. As in Fig. 4 (a), the dashed and dotted lines indicate where a single frequency band allows for a probability of unwrapping errors of 1% and 0.1%, respectively, and, accordingly, the arrows indicate where phase unwrapping could be performed with InSAR acquisitions in one or two frequency bands. Phase unwrapping errors lower than 1% are obtained with the described system for $B_F > 10\%$.

This approach is suitable to be used in a multi-band UAV

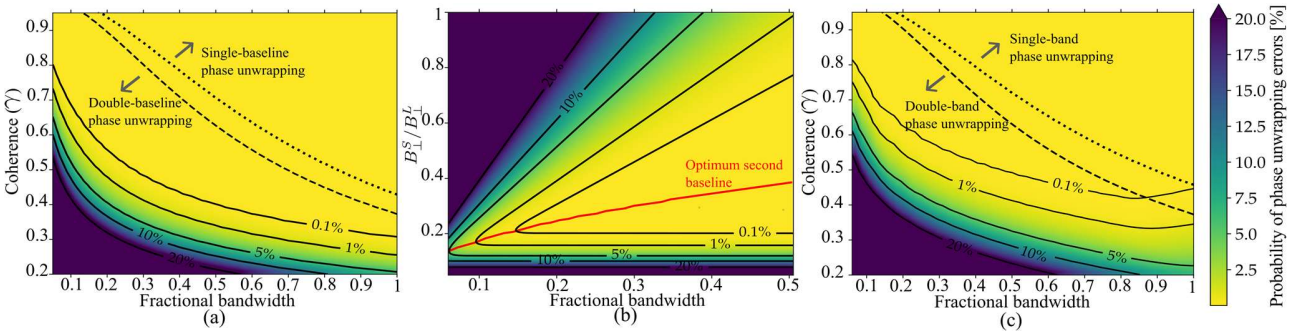

Fig. 4. (a) Probability of phase unwrapping errors versus B_F and the coherence when the unwrapping errors are corrected using a DEM from radargrammetry and one or two baselines. The dashed and dotted lines indicate where 1% and 0.1% of phase unwrapping errors are obtained with a single baseline, respectively. A multi-looking factor of 25 is considered. (b) Probability of phase unwrapping errors when a second acquisition with a smaller baseline is used as a function of B_F and the ratio between the smaller $B_\perp^S$ and larger $B_\perp^L$ perpendicular baselines. The red line shows the optimum baseline ratio. (c) Probability of phase unwrapping errors versus B_F and the coherence in a multi-band system with a secondary lower-band with $B_F = 0.2$. A multi-looking factor of 25 is assumed.

system since its applicability is not constrained by the need of specific baselines, which may be hard to achieve due to the low relative flying accuracy of UAVs [8], [10]. In the case of very distinct center frequencies, DEM calibration may be required to account for, e.g., the different ground penetration in each frequency band, similar to other multi-band approaches [19].

IV. Conclusions and Outlook

In this letter, a novel, generalized expression of the baseline decorrelation has been derived for wideband InSAR systems that allows achieving enhanced performance after spectral filtering. The new model includes the spectral shrinkage and is in good agreement with the simulations for both small and large bandwidths and baselines.

It was also shown that radargrammetry is useful for phase unwrapping in wideband InSAR systems because the height accuracies of both techniques become comparable. In addition to wideband drone- and airborne InSAR systems, the proposed approach could be employed, among others, in future spaceborne wideband X-band InSAR systems like HRWS $(B_{Rg} = 1.2\ \text{GHz}, B_F \approx 0.12)$ as well as in L-band systems such as Tandem-L $(B_{Rg} = 85\ \text{MHz}, B_F \approx 0.07)$ by increasing the multi-looking factor of the radargrammetric DEM [6], [20]. If a fractional bandwidth larger than 0.3 is available, performing phase unwrapping with a single InSAR acquisition becomes feasible. Furthermore, the proposed method is efficiently integrated in the processing chain without posing further constraints on the InSAR acquisition geometry.

The previous results were obtained by means of SAR data simulated over a uniform scene, which may differ from a real scenario with non-uniform scattering properties. Furthermore, the evaluation of the geometric decorrelation does not consider the roughness of the target nor subtle signal penetration, which have to be carefully considered in a real scenario due to the small heights of ambiguity. Our future work will utilize the presented concepts to generate accurate DEMs using experimental wideband UAV-based SAR acquisitions.

References

[1] A. Moreira et al., “A tutorial on synthetic aperture radar,” IEEE Geosci. Remote Sens. Mag., vol. 1, no. 1, pp. 6–43, Mar. 2013.

[2] R. Bamler and P. Hartl, “Synthetic aperture radar interferometry,” Inverse Problems, vol. 14, Art. no. 4, Aug. 1998.

[3] G. Krieger et al., “TanDEM-X: A Satellite Formation for High-Resolution SAR Interferometry,” IEEE Trans. Geosci. Remote Sens., vol. 45, Art. no. 11, Nov. 2007.

[4] P. A. Rosen et al., “Synthetic aperture radar interferometry,” Proceedings of the IEEE, vol. 88, Art. no. 3, Mar. 2000.

[5] F. Gatelli et al., “The wavenumber shift in SAR interferometry,” IEEE Trans. Geosci. Remote Sens., vol. 32, Art. no. 4, Jul. 1994.

[6] J. Mittermayer et al., "MirrorSAR: An HRWS Add-On for Single-Pass Multi-Baseline SAR Interferometry," in IEEE Trans. Geosci. Remote Sens., vol. 60, pp. 1-18, Art no. 5224018, Dec. 2021.

[7] R. Horn et al., "F-SAR — DLR's new multifrequency polarimetric airborne SAR," IEEE Int. Geosci. Remote Sens. Symp., Jul. 2009, pp. II-902-II-905.

[8] R. Bahnemann et al., “Under the sand: Navigation and localization of a micro aerial vehicle for landmine detection with ground-penetrating synthetic aperture radar,” Field Robotics, 2021.

[9] A. Ferretti et al., “InSAR Principles-Guidelines for SAR Interferometry Processing and Interpretation,” ESA Publications, Noordwijk, The Netherlands, Volume 19, 2007.

[10] M. Lachaise, T. Fritz and R. Bamler, "The Dual-Baseline Phase Unwrapping Correction Framework for the TanDEM-X Mission Part 1: Theoretical Description and Algorithms," in IEEE Trans.Geosci. Remote Sens., vol. 56, no. 2, pp. 780-798, Feb. 2018.

[11] R. Bamler and M. Eineder, "Split band interferometry versus absolute ranging with wideband SAR systems," IEEE Int. Geosci. Remote Sens. Symp., Sept. 2004, pp. 980-984 vol.2.

[12] C. Rossi, “Uncertainty assessment of single-pass TanDEM-X DEMs in selected applications,” Ph.D. dissertation, Institute of Photogrammetry and Cartography, Tech. Univ. of Munich, Munich, Germany, 2016.

[13] V. Mustieles-Perez et al., "Towards UAV-Based Ultra-Wideband Multi-Baseline SAR Interferometry," 2023 20th European Radar Conference (EuRAD), Berlin, Germany, 2023, pp. 233-236.

[14] H. A. Zebker and J. Villasenor, “Decorrelation in interferometric radar echoes,” in IEEE Trans. Geosci. Remote Sens., vol. 30, Art. no. 5, 1992.

[15] S. Kim, G. Krieger, and M. Villano, “Volume Structure Retrieval Using Drone-Based SAR Interferometry with Wide Fractional Bandwidth,” in Remote Sens. 2024, 16, 1352.

[16] M. Villano and K. Papathanassiou, “Differential shift estimation in the absence of coherence: performance analysis and benefits of polarimetry,” 5th Int. Workshop on Science and Applications of SAR Polarimetry and Polarimetric Interferometry, Frascati, Italy 2011.

[17] K. Kellogg et al., "NASA-ISRO Synthetic Aperture Radar (NISAR) Mission," 2020 IEEE Aerosp. Conf, Big Sky, MT, USA, 2020, pp. 1-21.

[18] M. T. Hallikainen et al., "Microwave Dielectric Behavior of Wet Soil-Part 1: Empirical Models and Experimental Observations," *in IEEE Trans. Geosci. Remote Sens., vol. GE-23, no*. 1, pp. 25-34, Jan. 1985.

[19] M. Pinheiro et al., "Generation of Highly Accurate DEMs Over Flat Areas by Means of Dual-Frequency and Dual-Baseline Airborne SAR Interferometry," in IEEE Trans. Geosci. Remote Sens., vol. 56, no. 8, pp. 4361-4390, Aug. 2018.

[20] G. Krieger and A. Moreira, “Multistatic SAR satellite formations: potentials and challenges,” in Proc. IEEE Int. Geosci. Remote Sens. Symp. (IGARSS), Nov., 2005, vol. 4, pp. 2680–2684.